RSC Advances

PAPER

View Article Online
View Journal | View Issue

Cite this: *RSC Adv.*, 2022, **12**, 26744

Nonlinear imaging and vibrational spectroscopic analysis of cellulosic fibres treated with COEX® flame-retardant for tapestry preservation†

Alice Dal Fovo, *[a] Jana Striova,[a] Diego Quintero Balbas, [a] Sara Mattana, [a] Niccolò Tacconi,[b] Riccardo Cicchi[a] and Raffaella Fontana[a]

Cellulose-based fabrics are widely used in the preservation and storage of historic tapestries. Their ease of flammability is a serious concern that greatly limits their applications and requires the development of effective and safe flame-retardant treatments. In this work, we analysed linen and cotton textile samples before and after COEX® treatment, a patented green technology imparting anti-flame properties by functionalizing the cellulose molecules with phosphorus and sulphur groups. Some of the samples were also exposed to photo-induced ageing after the treatment. The resulting structural and chemical changes in both fibres were characterized by nonlinear optical imaging modalities, namely Second Harmonic Generation (SHG) and Two-Photon Excited Fluorescence microscopies (TPEF), and Raman and Attenuated Total Reflection – Fourier Transform Infrared (ATR-FTIR) spectroscopies. Complementary results evidenced a reduction in microfibril crystallinity, attributed mainly to the reduction of hydrogen bonding among cellulose macromolecules, with a concomitant increase in fluorescence possibly due to the introduction of ester groups into cellulose chains and to decomposition of lignin into fluorescent by-products.

Received 13th April 2022
Accepted 24th July 2022

DOI: 10.1039/d2ra02384a

rsc.li/rsc-advances

Introduction

The ease of ignitability of textiles, when exposed to heat or flame, represents a severe concern that significantly limits their applications in several fields, including artwork conservation. Natural cellulose-based fabrics, which are extensively used in the preservation and conservation of historical tapestries,[1,2] are among the most flammable fibres, producing smoke and some toxic gases within combustion.[3,4] Since 1950, an increasing number of chemical treatments have been tested for low ignitability and flame propagation, as well as to inhibit the burning process of a wide range of polymeric materials, ranging from plastics and foams to synthetic or natural textiles.[5,6] However, in recent decades, some of the routinely applied flame-retardants (FRs), such as halogenates or phosphorus-based chemicals, have been proved to be persistent, bioaccumulative and toxic (so-called PBT chemicals) and, as in the case of brominated products, carcinogenic.[7,8] Therefore, research has been directed towards the development of safe and environment-friendly FRs with performances comparable to conventional compounds. Novel approaches involving nanostructures, *e.g.* organic–inorganic hybrid composites,[9] and biomacromolecules – mainly proteins and deoxyribonucleic acid[10] – have shown significant potential as novel green FRs. Nevertheless, the commercialization of hybrid flame-retardants and the most effective FR biomacromolecules is still restricted by the high cost of the processing technology.[9] Furthermore, many of the available biomacromolecules and bio-sourced products are highly soluble in water and thus not suitable for several textile applications.[10] The development of effective and harmless FRs that provide a sustainable and cost-effective alternative to current synthetic phosphorus and nitrogen products is attracting great interest.

Cellulosic fibres such as linen (or flax) and cotton are often used in tapestry conservation to consolidate and fill lacunae by sewing or reweaving some areas, to line or provide a new textile backing as a support, as well as to store and/or hang the tapestry. The widespread use of these fibres is due to their mechanical properties, which make them flexible enough to mould to the back of a tapestry and respond accordingly to environmental changes.[1,11]

As shown in Fig. 1, plant fibres consist of elongated cells of a cylindrical shape, with an outer primary cell wall (S1), an inner secondary cell wall (S2), and a hollow channel (lumen), running through the core of the fibre. S2, comprising microfibrils, accounts for the major portion of the elementary fibre's cross-section, and its main structural feature is a large content of crystalline cellulose. In cotton fibres, S2 is mainly composed of

[a]*Consiglio Nazionale delle Ricerche – Istituto Nazionale di Ottica (CNR-INO), Largo Enrico Fermi 6, 50125 Firenze, Italy. E-mail: alice.dalfovo@ino.cnr.it*

[b]*Università degli Studi di Firenze, Viale delle Idee 24, 50019 Sesto Fiorentino, Italy*

† Electronic supplementary information (ESI) available. See https://doi.org/10.1039/d2ra02384a

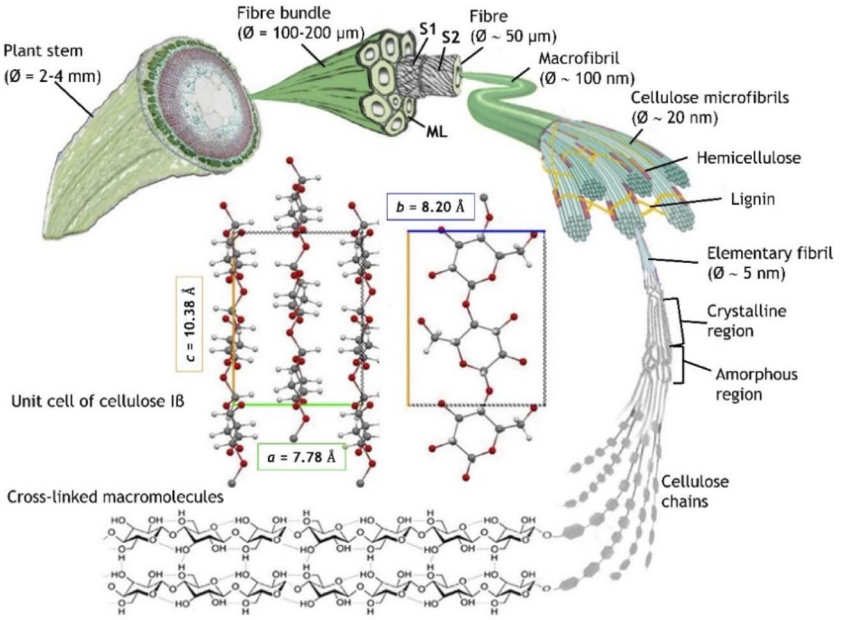

Fig. 1 Schematic representation of top-down cellulose hierarchical structure from its macroscopic origin, the plant stem (flax, in this representation). Cellulose microfibrils composing the secondary cell wall of fibres are coated with hemicelluloses, lignin, and pectins forming an interlocking matrix gel. The unit cell of cellulose Iβ, which is predominant in flax and cotton, is reported with *a*, *b*, and *c* lattice constants.

cellulose (around 95% of the weight), while less than 5% of the weight consists of waxes, protein, pectate and minerals.[12] The secondary wall in flax fibres exhibits a multi-layered structure in which crystalline cellulose (65–80% of the total weight) forms fibrils, oriented at 10° with the fibre axis, embedded in hemicellulose (up to 18%), pectins (up to 5%) and proteins (up to 3%).[13] The lignin content is 2–2.5%, whereas phenolics, waxes, fats, and minerals are present in an even lower percentage (1–1.5%).[14] The contact area and the hydrogen bonds between cellulose and hemicellulose, together with the covalent bonds in the backbone of the hemicellulose chain, determine the macro-mechanical behaviour of the fibres.[15,16] Single cellulose chains are aggregated in microfibrils by a net of hydrogen bonds conferring a crystalline or semi-crystalline structure with lattice parameters. Cellulose molecules can aggregate in a wide variety of secondary and tertiary structures bringing to a parallel or antiparallel organization and different chain polarity. These aspects influence the crystal parameters of the various allomorphs (crystalline phases) which in turn dictate the overall structural accessibility and the reactivity of cellulose.[17] The main portion (65–85%) of the fibres is crystalline (ordered region)[18] with the allomorph cellulose I naturally occurring in two distinct crystalline forms, Iα and Iβ, showing triclinic and monoclinic symmetry, respectively. Cellulose Iβ, which is predominant in flax and cotton,[19] is characterized by $a = 7.80$ Å, $b = 8.20$ Å, $c = 10.38$ Å lattice constants.[20] Hydrogen bonding is absent in smaller portion of the fibres resulting in amorphous (disordered) regions. Many physical and chemical treatments of cellulosic fibres target the hydroxyl groups in both the ordered and disordered regions causing changes in swelling and percentage crystallinity.

The COEX procedure (patent no. WO/2015/019272) used to impart the flame-retardant properties to the textile specimen studied here is described in detail in a patent. In brief, it consists of phosphorylation and sulphation of cellulose hydroxyl groups, thereby substantially reducing the number of free hydroxyl groups (Fig. 2).

In this work, we analysed linen and cotton textile samples, currently used in tapestry conservation for lining and storage of historical tapestries, before and after COEX® treatment. Some of the samples were also exposed to artificial ageing after the treatment.[21] This study builds on a knowledge about the properties of COEX treated textile samples gained through spectroscopic (molecular and elemental) methods, pH, flammability, water absorption and mechanical tests as described by Quintero Balbas *et al.*[21] Despite the verified flame-retardant properties, it was found that the COEX treated textile is affected by the loss of tensile strength of about 10% that is considered in some conservation context a critical factor. The goal of this study is to deepen the understanding of molecular and structural changes and verify their correlation with the observed reduction of mechanical properties. To this aim, we used a multi-analytical approach involving non-invasive and non-contact techniques: nonlinear optical imaging modalities, namely Second Harmonic Generation (SHG) and Two-Photon Excited Fluorescence (TPEF) microscopies, and Raman and Attenuated Total Reflection – Fourier Transform Infrared (ATR-FTIR) spectroscopies. The combination of microscopy imaging at submicron resolution and vibrational spectroscopic methods is ideal to investigate both the structural and chemical properties of plant tissues.[22] Here, we aimed to characterize the changes induced at

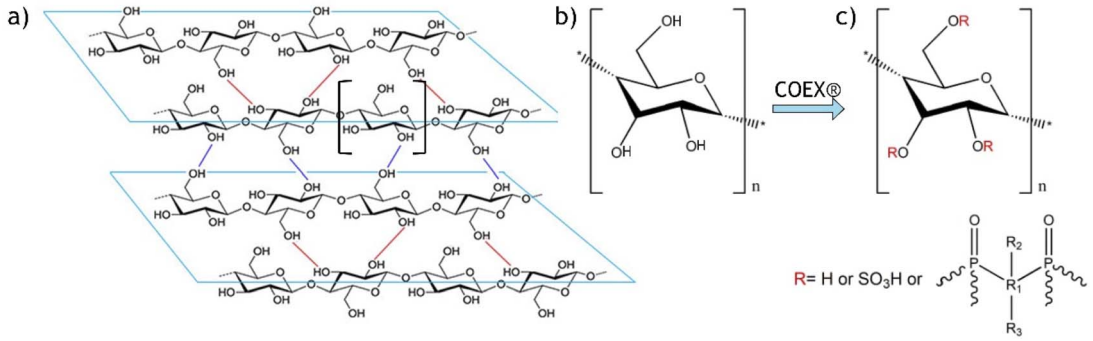

Fig. 2 Cellulose three-dimensional lattices cross-linked by hydrogen bonds (a) forming crystalline regions in microfibrils and monomer unit of cellulose before (b) after sulphation and phosphorylation (c) induced by COEX® treatment.

the molecular and microstructural level in the fibres following flame-retardant treatment and photo-induced ageing.

To date, studies of plant cells using nonlinear optical (NLO) imaging techniques are relatively few and mainly related to biological applications.[23–27] NLO imaging techniques have recently been introduced into the field of cultural heritage diagnostics for the characterization of an increasing variety of materials.[28] In particular, SHG and TPEF microscopy analysis of plant tissues and wood is still confined to laboratory samples[29] except for very few cases.[30,31]

SHG is a coherent nonlinear scattering process in which two low-energy photons interacting with a medium are up-converted to a single photon with twice the incident frequency (2ω). SHG signal is generated from dipolar interactions in materials having nonzero second-order susceptibility ($\chi(2)$), a requirement satisfied at the molecular scale by non-centrosymmetric molecules and highly-ordered nanostructures.[32] Being a coherent optical process, SHG is subjected to interference. Hence, the overall generated signal is significantly enhanced or suppressed according to the mutual phase relationship of individual emitters, which is in turn dependent on the ultrastructural organisation of the sample at the focal volume scale.[33] Cellulose is a non-centrosymmetric molecule and, thus, has the potential to produce SHG signal; a strong SHG signal has been observed from the crystalline region of cellulose microfibrils.[26] Starch, which is a mixture of amylose and amylopectin typically occurring in crystallites in a double helix structure in plant cells, generates a higher SH signal if compared with cellulose due to a lower symmetry of the glucose chain.[25,34]

TPEF, as another NLO process, requiring resonance with electronically excited states, adds selectivity for a broad range of fluorophores in plant cell that generates a strong autofluorescence signal. The main endogenous autofluorescent molecules in plants are chlorophyll and lignin, but there is a wide range of other molecules composing both cytoplasm and cell walls that are known to emit UV- or visible-excited fluorescence. Chlorophyll is excited by UV, blue or green light and emits strongly in the red spectral range (with maxima at 630 and 720–730 nm).[35] Lignin exhibits a characteristically broad emission range due to the presence of multiple fluorophore types, with maximum absorbance at 280 nm and a strong fluorescence emission centred at 360 nm, and a weaker visible fluorescence either UV-A or UV-B-excited.[36] It has been observed that fluorescence from lignin can also be generated through nonlinear absorption using a NIR excitation wavelength (840–860 nm).[29,30]

Materials and methods

Samples

We analysed eight textile samples of linen and cotton (average size 6.5 × 5.5 cm) reported in Table 1, provided by the Laboratory of Conservation of Tapestries and Carpets of the Opificio delle Pietre Dure in Florence (Italy) and currently used for the preservation of historical textiles, as previously described.[21] Samples were measured before and after the treatment with COEX® flame-retardant (Fig. 2). Artificial ageing was performed by exposing the textile samples T1AF, T1CA, T4AF, and T4CA to UV radiation (maximum emission at 254 nm and 312 nm, 30 W electric power) at 40 °C for 32 days.

Nonlinear optical microscopy (NLOM)

A detailed description of the nonlinear optical setup used in this study can be found elsewhere.[37] The system, based on a dual output fs-laser (Chameleon Discovery, Coherent Inc., Santa Clara, CA, USA), allows for multiple NLO contrast mechanisms, including TPEF, SHG, and coherent anti-stokes Raman scattering (CARS), and for fluorescence lifetime imaging microscopy (FLIM). The excitation wavelength was set at 800 nm, with a pulse duration of 100 fs and a repetition rate of 80 MHz. Nonlinear signals coming from the sample were epi-collected

Table 1 Analysed textile samples[a]

Flax samples	Cotton samples	Status
T1F	**T4F**	Not treated
T1FA	**T4FA**	Aged and not treated
T1C	**T4C**	COEX®-treated
T1CA	**T4CA**	COEX®-treated and aged

[a] A = aged; F = flammable (not treated); C = COEX®-treated.

using a Plan Apochromat 2010× objective lens (NA 0.7545, WD 2.1 mm, Nikon, Nikon Minato, Tokyo, Japan Carl Zeiss Microscopy, Jena, Germany) and detected with two photomultiplier tubes (H7422-40, Hamamatsu, Hamamatsu City, Japan) for simultaneous Two-Photon Excited Fluorescence (TPEF) and Second Harmonic Generation (SHG) detection. Signal was collected in the spectral range below 665 nm thanks to a dichroic filter (FF665-Di02, Semrock Inc. New York, NY, USA). A dichroic beam splitter with a 452 nm cutoff wavelength (FF452-Di01, Semrock Inc. New York, NY, USA) was used for the separation of TPEF and SHG. TPEF signal was transmitted and detected without any additional emission filter, in agreement with previous observations on TPEF emission spectral range of lignin.[30] The SHG signal was reflected and then filtered with a narrow band-pass filter centred at 400 nm (BrightLine 400/12–25 nm, Semrock Inc. New York, NY, USA). For each analysed area (field-of-view = 500 × 500 μm^2), both signals were detected and displayed as intensity images (resolution = 1024 × 1024 pixel), which were merged with a Java image processing software by assigning the TPEF and SHG images to the red and the green channel, respectively, to allow the visualization of both signals within the same image. The average power on the specimen was maintained at 30 mW for cotton samples and 40 mW for flax samples, with an acquisition time of about 10 seconds.

Sequentially shifted excitation Raman spectroscopy (SSE-RS)

Raman analysis was performed with a commercial handheld Raman spectrometer by Bruker (BRAVO), which allows for Sequentially Shifted Excitation Raman Spectroscopy (SSE-RS) using patented technology (SSE™, no. US8570507B1) to mitigate fluorescence. The device is equipped with two excitation lasers that can be temperature-shifted over a small wavelength range between 700 nm and 1100 nm to obtain sequential excitations with a separation of 6 cm^{-1}. For each measurement, six Raman spectra automatically acquired with an averaged spectral resolution of about 12 cm^{-1} are extracted and processed as described in the patent. The spectra are collected in two sequential spectral ranges (each covered by one of the two lasers), namely 170–2000 cm^{-1} and 2000–3200 cm^{-1}. Measurements are performed with a ~1 mm working distance and less than 100 mW laser power for both lasers. Here, we used 785 nm and 853 nm excitation wavelengths to acquire spectra in the range 170–3200 cm^{-1} over measurement areas of 0.05 mm^2 (01 × 0.5 mm^2). The spectra were acquired with 1000 ms acquisition time and 20 accumulations for the COEX samples and 2500 ms and 5 accumulations for the untreated samples. Based on NLO results, Raman analysis was performed on unaged samples only.

Attenuated total reflection – Fourier transform infrared spectroscopy (ATR-FTIR)

ATR-FTIR analyses were carried out with a Bruker Alpha spectrometer. The spectra in ATR mode (crystal diameter 4 mm) were recorded in the 400–4000 cm^{-1} range with 4 cm^{-1} spectral resolution. For each sample, we acquired 100 scans over five areas of a 12.5 mm^2. Data were processed with OPUS and Origin Pro software. Based on NLO results, we performed ATR-FTIR on unaged samples only.

Results

Nonlinear optical microscopy (NLOM)

Combined SHG/TPEF measurements were carried out on each textile sample in five areas of size 2.5 × 2.5 mm^2. Here we show a set of representative images for aged and unaged samples of flax and cotton, before and after the treatment with the flame-retardant. The mosaics of SHG/TPEF merged images reported in Fig. 3 are obtained by stitching 3 × 3 consecutive acquisitions (ROI 500 × 500 μm^2) over the sample surface. By assigning the TPEF and SHG signals to the red and green channels, respectively, the merged image allows visualization of the spatial distribution of SHG molecular emitters, *i.e.*, mainly cellulose and pectin, and nonlinear fluorescence emitters, *i.e.*, lignin and other autofluorescent species.

Nonlinear imaging on both unaged and aged samples shows that the green component corresponding to the SHG signal is attenuated after the COEX treatment, while the contribution of TPEF assigned to the red channel increases, especially in the unaged samples. In untreated flax fibres the SHG signal is generated by clusters of a few tens of microns (slightly more prevalent in unaged sample, T1F, than in the aged one, T1FA), which completely disappear in treated samples (T1C and T1AC), with a concomitant increase of fluorescence. A different distribution of the SH signal is observed in cotton fibres, where the green component uniformly overlaps the contribution of the fluorescence resulting in a green-yellow hue that appears particularly intense in T4F. After treatment, the red component attributed to fluorescence is predominant, especially in the unaged sample (T4C) which becomes orange, while the aged sample (T4AC) shows a more yellowish hue indicating a comparable contribution of both signals. The decrease of SH signal and increase in TPEF after treatment for both flax and cotton are indicative of a loss of microfiber crystallinity and a concomitant increase in fluorescence intensity due to the esterification of cellulose with the introduction of sulphate and phosphate functional groups. Indeed, inorganic cellulose esters, especially those containing aromatic moieties, are known to exhibit fluorescence properties.[38,39] The results of combined SHG/TPEF analyses also suggest that changes in nonlinear signals induced by artificial aging in cellulosic fibres are minimal (Fig. S1 in the ESI†). This is likely due to the material resistance towards the UV ageing, which did not induce any relevant change detectable by the proposed method. In terms of SHG and TPEF signal, the effect of flame-retardant treatment followed by ageing is comparable to that observed in the unaged sample, except for the increase in fluorescence, which is less evident in the aged samples (Fig. S2 in the ESI†). Based on these considerations, we focused the follow-up analysis on unaged samples only.

For a more detailed evaluation of the intensity variations of the SH and TPEF signals after flame-retardant treatment, we report the grey-scale images (Fig. 4) displaying the contribution

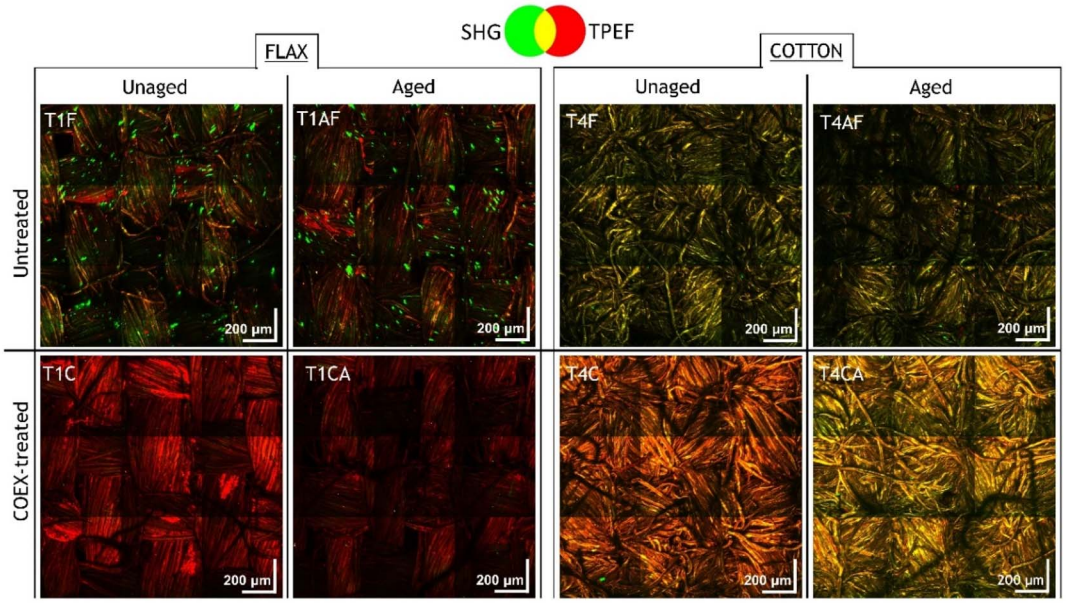

Fig. 3 Mosaics (1.5 × 1.5 mm^2) of nine SHG/TPEF merged images (500 × 500 µm^2, resolution 1024 × 1024 pixel) enabling the distinction between SHG (green-coded) and TPEF (red-coded) signals attributed to cellulose and lignin, respectively.

of SHG and TPEF signals as individual channels of the corresponding merged images (Fig. 3). For each fibre type, all images were acquired with 800 nm excitation wavelength under the same experimental conditions (objective lens, laser power, dwell time, target, detector gain, working distance, resolution, *etc.*) and as such are comparable to each other based on the signal intensity, which is expressed by the greyscale in the 8-bit images. The attenuation of SHG and the increase of TPEF are particularly evident in COEX®-treated flax sample (T1C), whereas the cotton sample (T4C) shows a consistent increase of fluorescence with an almost unchanged SH signal intensity. This would imply that the change in microfibre crystallinity is more significant in linen than in cotton.

Sequentially shifted excitation Raman spectroscopy (SSE-RS)

Raman analysis was performed on unaged samples of flax (T1) and cotton (T4), untreated (F) and treated (C) with the flame retardant. Raman spectra allowed for the distinction of characteristic cellulose bands, specifically the peaks at 1475 cm^{-1} and 380 cm^{-1} assigned to the allomorph 1β,[40] despite the strong fluorescence signal observed for both fibres after COEX® treatment (in agreement with what was observed in NLO

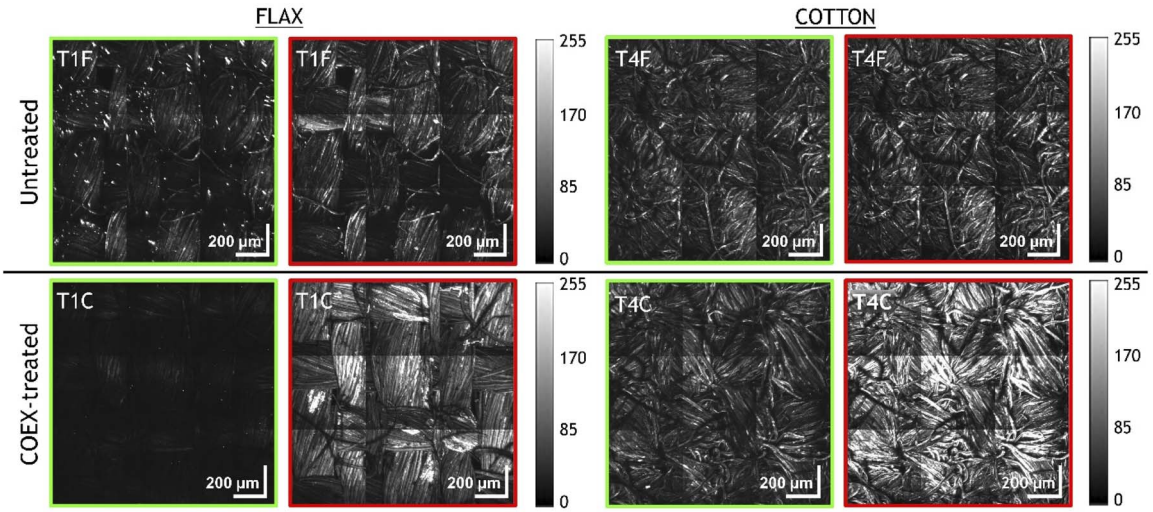

Fig. 4 SHG and TPEF images acquired on flax and cotton samples before (T1F, T4F) and after (T1C, T4C) the treatment. The 8-bit grey-scale images of red and green individual channels (red = SHG, and green = TPEF) show the contribution of SHG and TPEF signals, respectively, as image brightness in each pixel in the dynamic range 0–255.

analysis). Raw spectra of T1C and T4C reported in Fig. 5a and b exhibit a strong fluorescence background, which was then automatically removed by the SSE™ correction algorithm (Fig. 5c and d). No evident shifts in the position of the main peaks were detected after the treatment, meaning that no relevant changes in the molecular chains are produced. Specifically, the band assigned to the C–O–C glycosidic bonds and O6H group is present at 380 cm^{-1} in all spectra, as well as the band 1475 cm^{-1} CH_2OH exocyclic side chain of the allomorph Iβ, which is not shifted to lower wavenumbers, thus indicating that the group retains the tg conformation ($\chi = 180°$) after the treatment, in agreement with patent's claims. The spectra revealed the weak signal at ~1600 cm^{-1} assigned to the νsym phenyl ring of lignin compounds.[26]

We calculated the changes in crystallinity index (CrI) of cellulose according to the method proposed by Agarwal *et al.* for allomorph I,[41] which is based on the ratio between the intensity of the peaks at 380 cm^{-1} and 1096 cm^{-1}. These peaks are associated to the δ(CCC) ring bending in amorphous regions and to the asymmetric stretching of β-1,4-glycosidic linkages in crystalline regions, respectively. We also evaluated the organization of the molecular chains after the treatment based on the ratio between the intensity of the peaks attributed to the symmetric and asymmetric stretching of β-1,4-glycosidic linkages, *i.e.* 1121 cm^{-1} and 1096 cm^{-1}, respectively. The main results are reported in Table 2. The lower values of 380/1096 cm^{-1} and 1121/1096 cm^{-1} for T1C and T4C, compared with T1F and T4F, suggest that the treatment induces a reduction of both CrI and structural order. This can be ascribed to the partial loss of hydrogen bonds linking cellulose chains in the crystalline portion of microfibrils.

Table 2 Estimation of crystallinity and organization of cellulose macromolecules in flax and cotton samples before and after the treatment by ratiometric analysis of Raman peaks. Mean values calculated from 5 acquisitions are reported with the respective standard deviations

Sample	I^{380}/I^{1096} (STD)	I^{1121}/I^{1096} (STD)
T1F	0.6375 (0.0538)	0.5192 (0.0470)
T1C	0.6529 (0.0998)	0.4096 (0.0496)
T4F	0.7886 (0.0134)	0.6221 (0.0093)
T4C	0.7348 (0.0539)	0.6622 (0.0580)

Attenuated total reflection – Fourier transform infrared spectroscopy (ATR-FTIR)

The ATR-FTIR analysis on COEX®-treated samples (Fig. 6a) revealed the presence of newly-formed absorbance bands attributed to the treatment-induced reaction, *i.e.* the peaks at 1707 cm^{-1} and 813 cm^{-1} assigned to C=O and C–O–C, respectively. Additionally, we observed an increase in the relative intensities of the bands at 1426 cm^{-1} and in the range

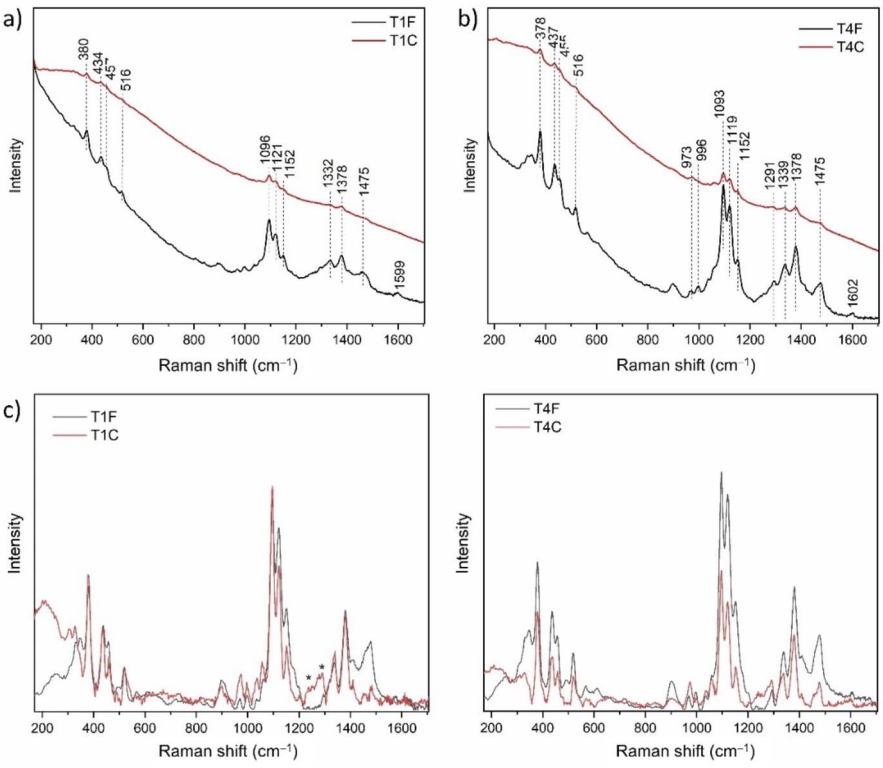

Fig. 5 Raman spectra of flax (T1) and cotton (T4) samples before (F) and after (C) the COEX® treatment; raw spectra (a and b) of the treated samples exhibit a strong fluorescence background, which is absent in the spectra (c and d) after the SSE™ correction. The asterisks indicate the peaks misidentified by the software that in all probability do not belong to the sample analysed.

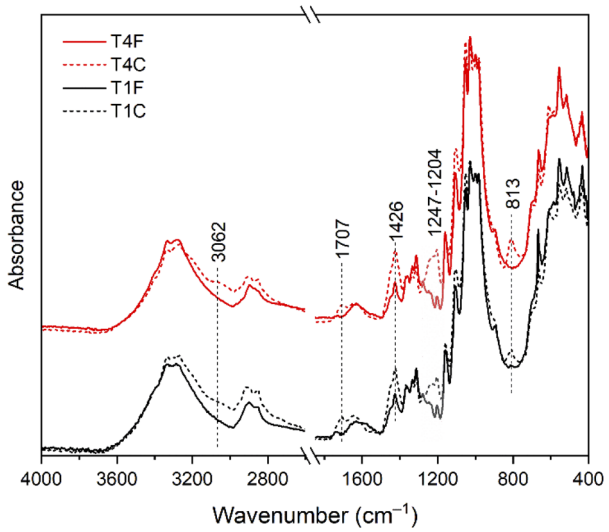

Fig. 6 FTIR analysis of treated (T1C, T4C) and untreated (T1F, T4F) samples highlighting the increase in the relative intensities of the bands at 1426 cm^{-1} and in the range 1204–1247 cm^{-1}.

1204–1247 cm^{-1}, the former attributed to the δCH_2 and the latter to νSO_2 and $\nu P{=}O$ groups. The band at 900 cm^{-1} also showed an increase in intensity, probably due to the formation of the P=O bonds. A further broad band with a maximum at 3062 cm^{-1} can be assigned to νCH_2. Some characteristic bands related to the physical and chemical changes, and specifically sensitive to the state of the crystalline and amorphous regions, are at 1372 cm^{-1} and 2900 cm^{-1}, respectively assigned to δCH and to νCH and νCH_2.[42] We used the ratio between 1372 cm^{-1} and 2900 cm^{-1} peak intensities to evaluate the crystallinity (Total Crystallinity Index, TCI) of the fibres after the treatment. The absorbance at 1372 cm^{-1} was measured using the minima at 1387 cm^{-1} and 1296 cm^{-1} as the baseline, whereas for the band at 2900 cm^{-1} we used the shoulder at 2978 cm^{-1} as the baseline. The TCI after the treatment resulted in a decrease of 0.1839 and 0.1319 for flax and cotton fibres, respectively (Table 3).

We also calculated the hydrogen-bond intensity (HBI) using the ratio between the absorbance bands at 3335 cm^{-1} and 1335 cm^{-1}, respectively assigned to the stretching and bending of the OH group, to quantify the crystallinity and regularity of cellulose molecules. We observed an increase of the HBI after the treatment of 0.4150 for flax and 0.0586 for cotton (Table 3), which is indicative of a lower crystallinity of the microfibrils.[43] We exclude that the higher HBI is related to the presence of water in fibres induced by the environmental RH because the samples were exposed to the same conditions throughout the measurements.

Table 3 Evaluation of the total crystallinity index (TCI) hydrogen-bond intensity (HBI) before and after the treatment based on 1372/2900 cm^{-1} and 3335/1335 cm^{-1} absorbance ratio, respectively. Mean values calculated from 5 acquisitions are reported with the respective standard deviation

Sample	TCI (STD)	HBI (STD)
T1F	0.99431 (0.08877)	3.09764 (0.31805)
T1C	0.81037 (0.07)	3.51268 (0.30869)
T4F	1.00182 (0.06754)	3.10769 (0.08771)
T4C	0.8699 (0.09984)	3.16632 (0.2033)

Discussion

The small reduction in microfibril crystallinity evidenced by both SHG/TPEF imaging and vibrational spectroscopy after COEX® treatment agrees with the declared percentage of OH substitution in cellulose chains (~2%). We do not exclude that the SHG signal observed in untreated samples is generated not only by crystalline cellulose but also by starch and specifically by amylopectin, whose glucose molecules are arranged in the same orientation, making the chains much less symmetrical than those of cellulose – where alternating glucose residues are instead arranged in reverse orientation. This means a stronger second-order nonlinear optical susceptibility and, therefore, more efficient SHG in starch than in cellulose. Especially in flax samples, the intense SHG signal likely emitted by starch agglomerates of a few tens of microns is no longer observed after treatment. This would imply that the COEX®-induced reaction might involve not only the crystalline regions of cellulose microfibrils, but also other polysaccharide macromolecules within the fibres. In addition, the absence of starch-related SHG signal after treatment may relate to the washing procedures aimed at removal of water-soluble and other compounds.

The concomitant increase in fluorescence detected by Raman and nonlinear techniques is consistent with the presence of newly formed FTIR bands attributed to treatment-induced esterification of cellulose chains, which nevertheless retain their orientation after treatment. As reported in the COEX® patent, the treatment may induce the decomposition of lignin into fluorescent byproducts, which would also cause an increase in fluorescence. Moreover, hemicellulose decomposition and lignin oxidation may induce the generation of fluorophores or reduced linkages between lignin and hemicellulose, resulting in increased fluorescence.[44] Some of these may be precursors for the chromophores responsible for the colour changes. This agrees with the measured colour values following the COEX treatment in these samples: ΔE of 2.8 and 5.1 respectively for T1C and T4C owed mainly to the increase of the b^* parameter (*i.e.*, yellowing).[21]

We hypothesize that the decrease in fluorescence observed after UV-exposure by SHG/TPEF imaging in treated samples is related to photo-induced degradation of the fluorescent moieties. Many possible deterioration processes can be detected by nonlinear optical imaging. Previous studies have demonstrated that SHG intensity can decrease not only because of disordering of cellulose (cellulose amorphization), but also due to the deterioration of the cellulosic fibres, and specifically, to enzymatic hydrolysis causing changes in cellulose supramolecular structure.[45] On the other hand, deterioration processes induced by weathering[46] and biological attack[47] may cause an

enrichment of the relative crystalline content at the expense of the amorphous fractions,[48] which would result in an increase of the SHG signal. Elucidating the effects of these degradation processes requires a systematic study that is beyond the scope of this article.

When dealing with esterification-based flame-retardant treatments, effective control of the degree of substitution, distribution and uniformity of the functional groups along cellulose chains is essential because a high degree of esterification causes significant depletion of the inter-chain hydrogen-bonding network, which severely affect the morphological and crystalline structure. Moreover, the reaction may occur either on the whole cellulose polymer chains to form cellulose esters or at the outer of cellulose fibres, thus leaving the interior cellulose crystalline structure in the interior intact.[38] The level of modification in cellulose nanocrystals can be, to some extent, qualitatively verified by examining the changes of crystallinity structure and morphology before and after the modification reactions. To this end, NLO imaging could be applied in combination with nuclear magnetic resonance to reveal key information about the chemical composition and structural features of macromolecules, while also providing quantitative data based on signals in NMR spectra.[49] This would also turn useful to characterize the chemical changes induced by deterioration processes, which is of utmost interest in the study of historical textiles and wooden artworks. By combining NMR with SHG/TPEF in depth analysis, the extent of micro-morphological changes can be investigated in all three spatial dimensions, allowing for a thorough characterization of cellulose-based materials.

Conclusions

The combined application of SHG/TPEF imaging and vibrational spectroscopic techniques suggests that COEX® treatment produces a reduction in microfibrils crystallinity, mainly attributed to the reduction of hydrogen bonding among cellulose macromolecules. Specifically, the attenuation of SHG signal is indicative of a loss of polarization anisotropy at both the molecular and ultrastructural level, whereas the increase of TPEF is possibly due to the introduction of ester groups into cellulose chains and to decomposition of lignin into fluorescent byproducts. The characteristic spectroscopic features of cellulose Iβ, which is the predominant allomorph in flax and cotton, were identified by both ATR-FTIR and Raman spectroscopies. The presence of newly formed absorbance bands attributed to treatment-induced esterification was also evidenced by FTIR, with a concurrent increase of fluorescence detected by Raman and nonlinear techniques. Despite those changes, both Raman and FTIR results confirm that cellulose chains maintain their orientation after the treatment.

The proposed analytical approach, combining NLO imaging and vibrational spectroscopic techniques, allows relating micrometric structural properties of flax and cotton fibres to the chemical changes induced by COEX®. This method, providing complementary information in a non-invasive way, is particularly suitable for artworks diagnostics and can be exploited to characterize the effects induced on textile fibres not only by anti-flame treatments, but also by deterioration processes.

Funding

This work was supported by Consiglio Nazionale delle Ricerche (CNR) [intervention program "CNR4C"] and the Regione Toscana [POR FSE 2014-2020 – Axis A Employment, "GiovaniSì"] as part of the projects SuperTec3D and RS4ART.

Author contributions

Conceptualization, J. S., R. C. and R. F.; methodology, J. S., R. C., R. F., A. D. F., D. Q. B. and S. M.; formal analysis, D. Q. B., S. M. and N. T.; data curation, D. Q. B., S. M. and A. D. F.; resources, R. F., J. S. and R. C.; writing – original draft preparation, A. D. F.; writing and editing, A. D. F.; review, R. F., R. C., J. S., D. Q. B. and S. M.; supervision, R. F., R. C. and R. F.; project administration, R. F. All authors have read and agreed to the published version of the manuscript.

Conflicts of interest

There are no conflicts to declare.

Acknowledgements

The authors thank conservators Claudia Cirrincione and Marta Cimò from the Opificio delle Pietre Dure and the COEX® Company, in particular, Simona Pesaro, Alberto Tonani, and Lucia Curioni, for providing the samples used in this research.

References

1 F. Lennard, *Stud. Conserv.*, 2006, **51**(suppl. 1), 43–53.
2 R. Costantini, F. Lennard, J. Alsayednoor and P. Harrison, *Eur. Phys. J. Plus*, 2020, **135**(6), 1–17.
3 D. Wesolek and R. Kozlowski, *Fire Mater.*, 2002, **26**(4–5), 215–224.
4 E. L. Vladimirtseva, S. V. Smirnova, O. I. Odintsova and M. V. Vinokurov, *Russ. J. Gen. Chem.*, 2016, **86**(2), 460–469.
5 Y. S. Kim, R. Davis, A. A. Cain and J. C. Grunlan, *Polymer*, 2011, **52**(13), 2847–2855.
6 T. A. Calamari Jr and R. J. Harper Jr, *Flame Retardants for Textiles*, Kirk-Othmer Encyclopedia of Chemical Technology, 2000.
7 P. O. Darnerud, *Environ. Int.*, 2003, **29**(6), 841–853.
8 G. Malucelli, F. Bosco, J. Alongi, F. Carosio, A. Di Blasio, C. Mollea and A. Casale, *RSC Adv.*, 2014, **4**(86), 46024–46039.
9 X. Wang, W. Guo, W. Cai, J. Wang, L. Song and Y. Hu, *Appl. Mater. Today*, 2020, **20**, 100762.
10 G. Malucelli, Biomacromolecules and bio-sourced products as flame retardants for textiles: a novel approach toward sustainability, *Green Chemistry for Sustainable Textiles*, Woodhead Publishing, 2021, pp. 27–55.
11 J. H. Hofenk de Graaff, F. Boersma and W. H. Roelofs, *Tapestry Conservation: Support Methods and Fabrics for*

Tapestries. Part I-II, Netherlands Institute for Cultural Heritage, Amsterdam, 1998.
12 M. Dochia, C. Sirghie, R. M. Kozłowski and Z. Roskwitalski, Cotton fibres, in *Handbook of Natural Fibres, Woodhead Publishing Series in Textiles*, ed. R. M. Kozłowski, Woodhead Publishing, 2012, pp. 11–23, ISBN no. 9781845696979.
13 J. G. Cook, *Handbook of textile fibres, I. Natural fibres*, Merrow, Durham, UK, 1993.
14 J. E. G. Van Dam and T. A. Gorshkova, *Encyclopedia of Applied Plant Sciences*, Elsevier, 2003, pp. 87–96.
15 L. I. Mikhalovska, V. M. Gun'Ko, A. A. Rugal, O. I. Oranska, Y. I. Gornikov, C. Morvan and S. V. Mikhalovsky, *RSC Adv.*, 2012, **2**(5), 2032–2042.
16 N. Zhang, S. Li, L. Xiong, Y. Hong and Y. Chen, *Modell. Simul. Mater. Sci. Eng.*, 2015, **23**(8), 085010.
17 U. P. Agarwal, *Molecules*, 2019, **24**(9), 1659.
18 D. V. Parikh, D. P. Thibodeaux and B. Condon, *Text. Res. J.*, 2007, **77**(8), 612–616.
19 A. Pakzad, J. Simonsen, P. A. Heiden and R. S. Yassar, *J. Mater. Res.*, 2012, **27**(3), 528–536.
20 P. Langan, N. Sukumar, Y. Nishiyama and H. Chanzy, *Cellulose*, 2005, **12**(6), 551–562.
21 D. Quintero Balbas, C. Cirrincione, M. Cimò, G. Lanterna, B. Pizzo, R. Fontana and J. Striova, *Polym. Degrad. Stab.*, 2022, **199**, 109907.
22 G. R. Littlejohn, J. C. Mansfield, J. T. Christmas, E. Witterick, M. D. Fricker, M. R. Grant and J. Love, *Front. Plant Sci.*, 2014, **5**, 140.
23 G. Mizutani, Y. Sonoda, H. Sano, M. Sakamoto, T. Takahashi and S. Ushioda, *J. Lumin.*, 2000, **87**, 824–826.
24 S. W. Chu, I. H. Chen, T. M. Liu, P. C. Chen, C. K. Sun and B. L. Lin, *Opt. Lett.*, 2001, **26**(23), 1909–1911.
25 G. C. Cox, N. Moreno and J. Feijo, *J. Biomed. Opt.*, 2005, **10**(2), 024013.
26 Z. Heiner, I. Zeise, R. Elbaum and J. Kneipp, *J. Biophotonics*, 2018, **11**(4), e201700164.
27 A. Melelli, F. Jamme, D. Legland, J. Beaugrand and A. Bourmaud, *Ind. Crops Prod.*, 2020, **156**, 112847.
28 A. Dal Fovo, M. Castillejo and R. Fontana, *La Rivista del Nuovo Cimento*, 2021, vol. 44, 9, pp. 453–498.
29 A. Dal Fovo, S. Mattana, M. Marchetti, M. Anichini, A. Giovannelli, E. Baria, R. Fontana and R. Cicchi, *Photonics*, 2022, **9**, 170.
30 G. Latour, J. P. Echard, M. Didier and M. C. Schanne-Klein, *Opt. Express*, 2012, **20**(22), 24623–24635.
31 A. Melelli, G. Roselli, N. Proietti, A. Bourmaud, O. Arnould, F. Jamme and C. Santulli, *Journal of Cultural Heritage*, 2021, **52**, 202–214.
32 P. J. Campagnola, A. C. Millard, M. Terasaki, P. E. Hoppe, C. J. Malone and W. A. Mohler, *Biophys. J.*, 2002, **82**(1), 493–508.
33 R. M. Brown Jr, A. C. Millard and P. J. Campagnola, *Opt. Lett.*, 2003, **28**(22), 2207–2209.
34 V. Nessi, A. Rolland-Sabaté, D. Lourdin, F. Jamme, C. Chevigny and K. Kansou, *Carbohydr. Polym.*, 2018, **194**, 80–88.
35 L. Donaldson, *Molecules*, 2020, **25**(10), 2393.
36 K. Radotić, A. Kalauzi, D. Djikanović, M. Jeremić, R. M. Leblanc and Z. G. Cerović, *J. Photochem. Photobiol., B*, 2006, **83**(1), 1–10.
37 M. Marchetti, E. Baria, R. Cicchi and F. S. Pavone, *Methods Protoc.s*, 2019, **2**(2), 51.
38 Y. Wang, X. Wang, Y. Xie and K. Zhang, *Cellulose*, 2018, **25**(7), 3703–3731.
39 J. Zhang, W. Chen, Y. Feng, J. Wu, J. Yu, J. He and J. Zhang, *Polym. Int.*, 2015, **64**(8), 963–970.
40 M. Makarem, C. M. Lee, K. Kafle, S. Huang, I. Chae, H. Yang and S. H. Kim, *Cellulose*, 2019, **26**(1), 35–79.
41 U. P. Agarwal, R. S. Reiner and S. A. Ralph, *Cellulose*, 2010, **17**(4), 721–733.
42 S. Y. Oh, D. I. Yoo, Y. Shin and G. Seo, *Carbohydr. Res.*, 2005, **340**(3), 417–428.
43 M. Poletto, A. J. Zattera and R. M. Santana, *J. Appl. Polym. Sci.*, 2012, **126**(S1), E337–E344.
44 H. C. Tai, P. L. Chen, J. W. Xu and S. Y. Chen, Two-photon fluorescence and second harmonic generation hyperspectral imaging of old and modern spruce woods, *Opt. Express*, 2020, **28**(26), 38831–38841.
45 A. Peciulyte, J. Kiskis, P. T. Larsson, L. Olsson and A. Enejder, *Cellulose*, 2016, **23**(3), 1521–1536.
46 F. Lionetto, R. Del Sole, D. Cannoletta, G. Vasapollo and A. Maffezzoli, *Materials*, 2012, **5**(10), 1910–1922.
47 C. Howell, A. C. S. Hastrup, B. Goodell and J. Jellison, *Int. Biodeterior. Biodegrad.*, 2009, **63**(4), 414–419.
48 P. Budrugeac and A. Emandi, *J. Therm. Anal. Calorim.*, 2010, **101**(3), 881–886.
49 Y. Zhao, Y. Man, J. Wen, Y. Guo and J. Lin, *Trends Plant Sci.*, 2019, **24**(9), 867–878.